Pyrene Cholesterol Reports the Transient Appearance of Nonlamellar Intermediate Structures during Fusion of Model Membranes†

Vladimir S. Malinin‡ and Barry R. Lentz*,§

Elan Pharmaceuticals, 1 Research Way, Princeton, New Jersey 08540, and Department of Biochemistry & Biophysics, CB#7260, University of North Carolina at Chapel Hill, Chapel Hill, North Carolina 27599-7260

Received October 12, 2001; Revised Manuscript Received February 19, 2002

ABSTRACT: We have hypothesized that modulating the free energy of hydrophobic mismatch (HM) might be a principal means to control the fusion process and that it may be a role of cholesterol to counteract HM and make membranes fusogenic. To test these hypotheses, we examined the ability of cholesterol 1-pyrenebutyrate (PY-Ch) and other pyrene-containing fluorescent probes to report interstices formed during the $L_\alpha-H_{II}$ transition of DiPoPE in terms of changes in excimer/monomer (E/M) fluorescence ratios. We found a significant (>150%) increase in the PY-Ch E/M in the hexagonal phase relative to the lamellar phase, presumably resulting from redistribution of PY-Ch from the curved lamellar leaflets to coexisting HMs that constitute 20 vol % of this phase. All other probes showed a much smaller or even an opposite (PY-hexadecanoic acid) effect. The time course of the PY-Ch E/M ratio during fusion of DOPC/PE/Ch small unilamellar vesicles showed a transient increase with a subsequent decrease, consistent with fusion proceeding through intermediates with significant HM. The amplitude and position of the maximum in E/M correlated with the rate of contents mixing. An increase in E/M was not seen when lipid mixing occurred in the absence of contents mixing. Our results suggest that PY-Ch provides a tool for monitoring fusion intermediates that occur after the initial fusion intermediate but prior to pore formation, possibly by accumulating in regions associated with HM.

Membrane fusion, although driven by fusion proteins, is commonly understood to be lipidic in nature (*13*). It can be defined in general as a process that transforms opposed lipid bilayers between two topologically distinct states in which previously distinct and unconnected trapped compartments become connected by an aqueous path. Membrane fusion is often modeled as a sequence of lipidic intermediates (*4*, *12*, *21*), some of which are essentially nonlamellar. The incompatibility of lamellar and nonlamellar intermediate structures necessarily leads to inhomogeneities in packing that raise the free energy of the intermediate relative to the lamellar phase. When the fusion intermediate structure is modeled in terms of bent monolayers of constant thickness, this packing inhomogeneity is revealed as an empty space between hydrophobic surfaces, the so-called "hydrophobic void" (*21*). Clearly, a "void" exists only as a convenient construct in this simplified model. In reality, lipids must somehow accommodate their preferred lamellar structure to reduce this mismatch of coexisting lipid structures. Acyl-chain stretching (*7*), lipid-tilting (*6*), or other types of phospholipid packing distortion (*25*) have been proposed to achieve this accommodation. To avoid the assumptions of any particular proposal, we prefer to use a more general term, "hydrophobic mismatch" (HM),[1] to describe the existence of packing inhomogeneity within specific regions of fusion intermediate structures. Since any accommodation of lamellar structures to lower the free energy of the HM will raise the free energy of the lamellar structures, one way or another, the additional free energy associated with formation of a HM is likely to provide a barrier to formation of fusion intermediates and thus to the fusion process. Based on the complementary fusion-enhancing effects of osmotic stress and short-chain hydrocarbons, we have proposed recently that the free energy of HM formation may be a major term opposing formation of the committed intermediate leading to membrane fusion, and that modulating this energy might be a way to regulate fusion (*16*). In the current work, we take the first step toward testing whether HM formation modulates fusion by developing an assay, based on the behavior of fluorescent probes during hexagonal phase formation, to monitor the appearance of nonlamellar intermediates during lipid vesicle fusion.

MATERIALS AND METHODS

1,2-Dioleoyl-*sn*-glycero-3-phosphocholine (DOPC[1]), 1,2-dipalmitoleoyl-*sn*-glycero-3-phosphoethanolamine (DiPoPE[1]), 1,2-dioleoyl-*sn*-glycero-3-phosphoethanolamine (DOPE[1]), and 1-stearyl-2-oleoyl-*sn*-glycero-3-phosphocholine (SOPC[1]) were purchased from Avanti Polar Lipids, Inc. (Birmingham,

† Supported by USPHS Grant GM32707 to B.R.L.

* To whom correspondence should be addressed. E-mail: uncbrl@med.unc.edu.

‡ Elan Biopharmaceuticals.

§ University of North Carolina at Chapel Hill.

[1] Abbreviations: Ch, cholesterol; DOPC, 1,2-dioleoyl-*sn*-glycero-3-phosphocholine; SOPC, 1-stearyl-2-oleoyl-*sn*-glycero-3-phosphocholine; DOPE, 1,2-dioleoyl-*sn*-glycero-3-phosphoethanolamine; DiPoPE, 1,2-dipalmitoleoyl-*sn*-glycero-3-phosphoethanolamine; E/M, excimer/monomer ratio; HM, hydrophobic mismatch; PEG, poly(ethylene glycol); SUV, small, unilamellar vesicles made by sonication technique; PY-Ch, cholesteryl 1-pyrenebutyrate; PY-PE, 1-hexadecanoyl-2-(1-pyrenedecanoyl)-*sn*-glycero-3-phosphoethanolamine; PY-DA, 1-pyrenedecanoic acid; PY-HDA, 1-pyrenehexadecanoic acid.

10.1021/bi011924h CCC: $22.00
Published on Web 04/16/2002

AL), and used without further purification. Cholesterol (from Avanti Polar Lipids) was purified via the dibromide form (*20*). Concentrations of phospholipid stocks in chloroform were determined by phosphate assay (*2*). Cholesteryl 1-pyrenebutyrate (PY-Ch), 1-hexadecanoyl-2-(1-pyrenedecanoyl)-*sn*-glycero-3-phosphoethanolamine (PY-C10-HPE), 1-pyrenedecanoic acid (PY-DA), and 1-pyrenehexadecanoic acid (PY-HDA) were purchased from Molecular Probes (Eugene, OR). Dodecyl octaethylene glycol monoether detergent (C12E8[1]) was purchased from Calbiochem (LaJolla, CA). PEG of molecular weight 7000−9000 (PEG 8000) was purchased from Fisher Scientific (Fairlawn, NJ) and purified as described previously (*14*). Polybead polystyrene microspheres were purchased from Polysciences, Inc. (Warrington, PA). All other reagents were of the highest quality available.

Vesicle Preparation. A volumetrically measured mixture of appropriate lipids and probes in chloroform was dried under a stream of nitrogen. The dried lipids were dissolved in cyclohexane with an aliquot of methanol (about 5 vol %), frozen on dry ice, and lyophilized under high vacuum overnight. The lyophilized lipids were suspended with occasional agitation in an appropriate buffer for about 1 h at room temperature at a concentration of 10 mM. The fusion buffer contained 100 mM NaCl, 10 mM TES, 1 mM EDTA, pH 7.4. Small unilamellar vesicles (SUV[1]) were prepared as previously described (*11*). The lipid suspension was sonicated for 10 min using a Heat Systems model 350 Sonicator (Plainview, NY) equipped with a titanium probe tip of 9.5 mm diameter. After sonication, the sample was fractionated by centrifugation at 70 000 rpm for 25 min at 4 °C using a Beckman TL-100 ultracentrifuge (Palo Alto, CA) (*1*).

Contents Mixing and Leakage Assays. Tb^{3+}/DPA contents mixing and leakage assays (*26*) were adapted to perform kinetic measurements. For the contents mixing assay, two populations of vesicles were used, one encapsulating Tb^{3+} buffer (8 mM $TbCl_3$, 60 mM sodium citrate, 10 mM TES), and another DPA buffer (80 mM DPA, 10 mM TES, pH 7.4). In leakage experiments, vesicles prepared in Tb^{3+}/DPA buffer (4 mM $TbCl_3$, 30 mM sodium citrate, 40 mM DPA, 10 mM TES, pH 7.4) were used. Untrapped buffer was removed using a Sephadex G-75 column equilibrated with fusion buffer, which had the same osmolality as the trapped buffer.

The contents mixing assay was carried out by mixing equal amounts of vesicles (0.1 mM lipid) containing either $TbCl_3$ or DPA in a fusion buffer with an appropriate volume of PEG solution. The resulting increase in fluorescence intensity due to formation of the Tb/DPA complex was recorded using an SLM 48000 MHF spectrofluorometer (SLM Instruments, Rochester, NY) with an excitation wavelength of 278 nm (slit = 4 nm). A monochromator set to a wavelength of 545 nm (slit = 32 nm) along with a cutoff filter (OG500, Schott Glass Technologies, Duryea, PA) were used to define the emitted light. The percent of contents mixing at each particular PEG concentration was calculated based on the assumption that 100% contents mixing corresponded to the fluorescence of vesicles containing both $TbCl_3$ and DPA (Tb/DPA vesicles, representing fusion of one Tb^{3+} vesicle to one DPA vesicle) (*24*).

Percent leakage was calculated from the drop in fluorescence of Tb/DPA vesicles upon addition of PEG, where 100% leakage was characterized as the fluorescence following addition of $C_{12}E_8$ detergent at a concentration of 1 mM (*24*). This measurement was used to correct contents mixing readings for the fraction of contents that leaked during mixing with PEG, making the contents mixing assays fairly insensitive to leakage up to about 50% leakage (*24*). This correction is important since leakage, while a process distinct from fusion, often occurs under conditions very similar to those that trigger fusion (*15*, *18*).

Lipid Mixing Assay. For measuring lipid mixing, we used an assay based on resonance energy transfer between lipid-attached fluorescent probes BODIPY500-PC and BODIPY530-PE (*17*). Vesicles labeled with 0.5 mol % of each probe were mixed with probe-free vesicles at a 1:4 ratio (final lipid concentration of 0.2 mM). The appropriate amount of PEG solution was added, and the change of donor to acceptor fluorescent intensity ratio, due to probe dilution, was recorded. The percent of lipid mixing was calculated according to the equation:

$$\%\ \mathrm{LM} = \frac{(L/P)/(L/P)_o - 1}{n} \times 100 \qquad (1)$$

using a calibration curve obtained from measurements with several L/P ratios in SUVs of the same composition. Here L/P is the lipid to probe ratio, $(L/P)_o = 200$ is the original lipid to probe ratio in the probe-containing population, and $n = 4$ is the ratio of probe-free vesicles to probe vesicles. BODIPY500-PC was excited at 500 nm, and the emission intensities of donor and acceptor were recorded in channel A at 520 nm and in channel B using a 550 nm cutoff filter OG550 (Schott Glass Technologies), respectively.

Pyrene Excimer Formation Fluorescent Measurements. Fluorescence was recorded using the SLM 48000 MHF spectrofluorometer operating in the T format. The sample was excited at 345 nm with narrow slits (0.5 nm) and a bandpass filter (UG11, Schott Glass Technologies) centered at 340 nm, with a 50 nm bandwidth. The monomer intensity was measured in channel A through a monochromator set to a wavelength of 396 nm (slits = 16 nm), and the excimer intensity was measured simultaneously in channel B using a cutoff filter (GG475, Schott Glass Technologies). The settings were chosen to reduce photobleaching during long-term measurements and to eliminate detection of scattered (or reflected) light of higher wavelengths coming from overtones of the principle setting of the excitation monochromator. Pyrene-labeled lipids were used at a concentration of 0.5 mol % in the two different processes studied, fusion of SUVs or interconversion of lamellar and hexagonal phases of DiPoPE. In both cases, special precautions were taken to reduce unwanted signal fluctuations due to sample inhomogeneity and/or change of optical properties associated with the processes observed. Thus, we recorded the ratio of excimer to monomer fluorescence measured simultaneously in two channels. The change in signal due to sample optical fluctuations would be similar in both channels, and taking the ratio of signals eliminated a great deal of scatter presumably due to this effect.

Lamellar to Hexagonal Phase Transition Detection. Lyophilized DiPoPE with 0.5 mol % of PY-containing probe

(total lipid amount 30 μmol) was hydrated in 1.5 mL of fusion buffer for 1 h at room temperature. The suspension was freeze/thawed 5 times (dry ice/30 °C water bath) and then centrifuged for 30 s at 1000*g*. The excess buffer was removed, and the lipid-rich fraction was loaded into ACCU-FILL 90 MICROPET capillaries (0.8/1.2 mm internal/external diameter, Clay Adams, Parsippany, NJ). The capillaries were sealed with Critoseal (Oxford Labware, St. Louis, MO) and stored at 4 °C for a period not more than 5 days. All procedures except centrifugation were performed under a nitrogen atmosphere to ensure complete oxygen removal.

For fluorescence measurements, a capillary containing the lipid sample was centered in an optical cuvette filled with water. Water significantly reduced light reflection from the water−glass interface, so that the light coming to the photodetectors was mostly the fluorescent emission of pyrene-containing probes from the thin layer of the sample near the wall of the glass capillary. Separate experiments with probe-free samples showed that light scattering and/or reflection produced less than 2% of the total signal in each channel.

Temperature scans were performed using a thermostated, circulating water-bath (K-2/R; Brinkmann Instruments). For temperature scanning, the temperature setting was changed to a value above (for heating) or below (for cooling) the range used in the experiment, and the bath was allowed to heat or cool, respectively. Temperature was measured with a Digitec thermo-probe (United Systems Corp., Dayton, OH) in an identical cuvette filled with water and placed in the same four-position cuvette holder. The scan rate was usually in the range of 15−25 °C/h, with an average of around 20 K/h.

RESULTS

Pyrene Excimer Formation in the DiPoPE Hexagonal Phase. We checked several pyrene-containing fluorescent probes for their ability to reflect formation of the hexagonal phase of DiPoPE (Figure 1). The excimer/monomer ratio (E/M) generally increases with increasing temperature due to increased diffusion and hence collision rate between probes. At temperatures around 40 °C, the E/M ratio underwent a sudden shift to a different level or a dramatic change in slope. If presented as the derivative of the E/M, this behavior appeared as well-defined peaks (see inset in Figure 1A). By these procedures, all four probes reported in heating scans a transition temperature (40.3−41.0 °C) close to that detected in heating differential scanning calorimetry scans or X-ray diffraction measurements of the $L_\alpha-H_{II}$ phase transition of pure DiPoPE (41.5−43 °C) (*5*, *23*). In cooling scans, the phase transition occurred at lower temperature, showing a well-defined hysteresis. Because of this hysteresis, there was a range of temperatures over which the lamellar phase existed in the heating experiment and the hexagonal phase existed in the cooling experiment. To contrast the E/M ratios in the hexagonal and lamellar phases, we compared the E/M ratios at the temperature equidistant from the heating and cooling peaks (T_{H2} and T_{H1}, see Figure 1A). On the basis of this criterion, PY-CH showed the greatest increase in excimer formation in the hexagonal relative to the lamellar phase. This difference exceeded 150% of the original E/M ratio in

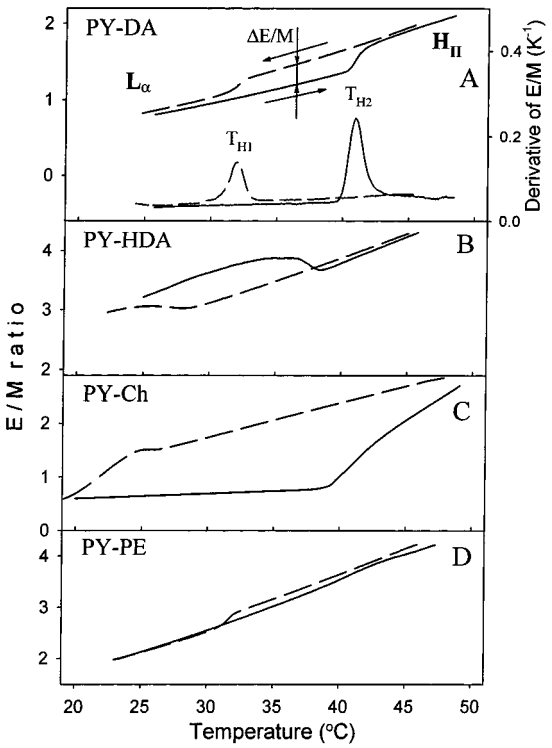

FIGURE 1: Temperature scans of fluorescence of pyrene-labeled probes in DiPoPE. Excimer to monomer fluorescence ratios as a function of temperature collected in heating (solid lines) and cooling (dashed lines) scans for pyrene-labeled probes PY-DA (A), PY-HDA (B), PY-Ch (C), PY-PE (D). Arrows show the directions of temperature scans. Temperature derivatives of the PY-DA curves in panel A are shown to illustrate how we determine phase transition temperatures. Peaks indicate the position of the $L_\alpha-H_{II}$ phase transition for heating (T_{H2}) and cooling (T_{H1}) scans.

the lamellar phase (heating scan) and indicated that PY-Ch collected in a smaller volume or diffused more rapidly in the hexagonal versus the lamellar phase. The E/M ratio of PY-DA also increased in the hexagonal phase, indicating that it too clustered or diffused more rapidly in this phase. In contrast to the behavior of PY-Ch and PY-DA, the E/M ratio of PY-PE showed no significant change through the lamellar−hexagonal phase transition, indicating that this probe behaved similarly in the hexagonal phase as in the lamellar phase. Finally, the E/M ratio of PY-HDA acid surprisingly decreased in the hexagonal phase relative to the lamellar phase, indicating that the pyrene moieties are closer together in the lamellar phase than in the hexagonal phase. This could be because the length of this fatty acid would place the pyrene group roughly in the center of the lamellar phase, making its concentration per unit area twice that to be expected if it were confined, as for the other probes, to individual leaflets of the bilayer.

The near-agreement of scanning calorimetry and X-ray scattering transition temperature (*5*, *23*) suggests that the hysteresis observed for the DiPoPE $L_\alpha-H_{II}$ phase transition derives mostly from a slow H_{II} to L_α transition rather than a slow L_α to H_{II} transition. Despite a fairly low probe concentration (0.5 mol %), the temperature of the lamellar−hexagonal phase transition detected in cooling scans was affected by the presence of the different fluorescent probes, suggesting that the presence of different probes affected the rate of the H_{II} to L_α transition differently. PY-Ch had the greatest effect in cooling scans, lowering T_{H1} to 22 °C

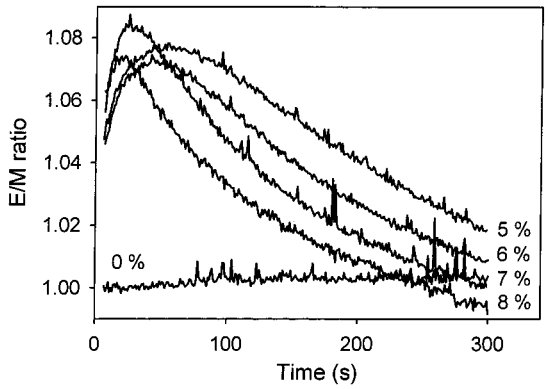

FIGURE 2: Fluorescence of PY-Ch in DOPC/DOPE/Ch SUVs during PEG-induced fusion. Excimer-to-monomer ratio was recorded as a function of time following PEG addition at different concentrations to SUVs (0.2 mM; 0.5 mol % PY-Ch) at 23 °C and normalized to the value in a control sample without PEG.

compared to about 32 °C for PY-PE and PY-DA. This implies that PY-Ch had the greatest effect either in raising the free energy barrier that links the H_{II} phase to the L_α phase or in stabilizing the H_{II} phase relative to these intermediate structures.

Pyrene Cholesterol Excimer Formation during PEG-Induced Vesicle Fusion. The cross section of a hexagonal phase has very negatively curved lamellar arrangements coexisting with large regions (20 vol %) of HM, a lipid arrangement very similar to the hypothetical structure of fusion intermediates, especially the trans-membrane complex (TMC) (*23*). For this reason, we would expect that the pyrene-containing probes we have examined might partition similarly between lamellar structures and HM regions in fusing membranes as in the hexagonal phase. We recorded the PY-Ch E/M ratio during PEG-mediated fusion of DOPC/DOPE/Ch 2/1/1 SUVs. The data presented in Figure 2 show that, upon addition of different concentrations of PEG, excimer fluorescence always increased through a maximum and then decreased as fusion proceeded. As a control, the PY-Ch E/M ratio was measured after addition of buffer without PEG (flat curve marked 0% in Figure 2). Pyrene fluorescence is quite sensitive to temperature, so in order to minimize artifacts due to temperature changes, we preincubated buffer and PEG solutions at the temperature of the vesicle sample before mixing these with vesicles. If we followed this precaution, then the signal from the control was constant within 0.5% during the time course of fusion. The PEG-induced change in E/M ratio usually did not exceed 10% of the control value but could easily be measured with good accuracy.

To examine the relationship of different events during fusion to the E/M ratio, we compared the Py-Ch E/M ratio as well as lipid mixing and contents mixing during PEG-mediated fusion of vesicles of different lipid compositions (DOPC/DOPE/Ch, DOPC/DOPE, SOPC). The results are recorded in Figure 3. DOPC/DOPE/Ch SUVs were most fusogenic and showed both contents mixing and lipid mixing. PY-Ch in these vesicles also formed excimers most readily as evidenced by the increase in E/M ratio (Figure 3A). After reaching a maximum, the E/M ratio slowly decreased toward a value characteristic of nonfusing vesicles. DOPC/DOPE vesicles do not fuse at the PEG concentration used for this series of experiments (5 wt %) but do form hemifusion

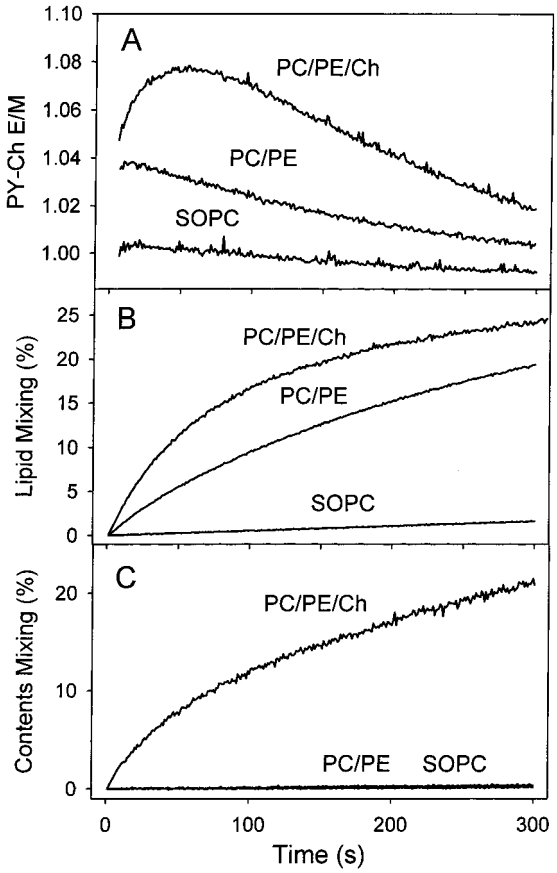

FIGURE 3: Pyrene excimer formation correlates with contents mixing but not with lipid mixing. The time courses of changes in E/M ratio of SUVs containing 0.5 mol % PY-Ch (A) and lipid mixing (B) and contents mixing (C) after addition of 5 wt % PEG are shown for vesicles of different compositions (DOPC/DOPE/Ch 2/1/1, DOPC/DOPE 3/1, and SOPC), as indicated on the plot. The E/M ratios were normalized for each lipid composition with respect to a control lacking PEG.

complexes as evidenced by a substantial rate of lipid mixing (Figure 3B). For DOPC/DOPE vesicles, the pyrene E/M ratio increased more rapidly than we could measure but then decreased slowly toward the value seen for the nonfusing, nonlipid-mixing control vesicles (SOPC). From these results, one can conclude that an initial and very rapid increase in the PY-Ch E/M ratio correlated with formation of a structure that leads to lipid mixing. A slower increase in the E/M ratio through a maximum correlated with formation of an intermediate structure that leads to contents mixing or fusion. The PY-Ch E/M ratio decreased with time as lipid mixing or fusion proceeded in all cases, indicating that these structures disappeared as the fusion or lipid mixing processes concluded.

The most reproducible aspect of the pyrene E/M ratio time courses shown in Figure 2 was the position of the maximum. Higher PEG concentrations induced more rapid change in excimer formation and shifted the maximum to shorter time. We compare in Figure 4 the position of this maximum to the initial rate of contents mixing observed at these different PEG concentrations. There was clearly a remarkable correlation between the rate of contents mixing and the reciprocal of the position of the E/M maximum. This reinforces our conclusion that the increase in PY-Ch E/M ratio marks formation of an intermediate structure leading to formation of a fusion pore.

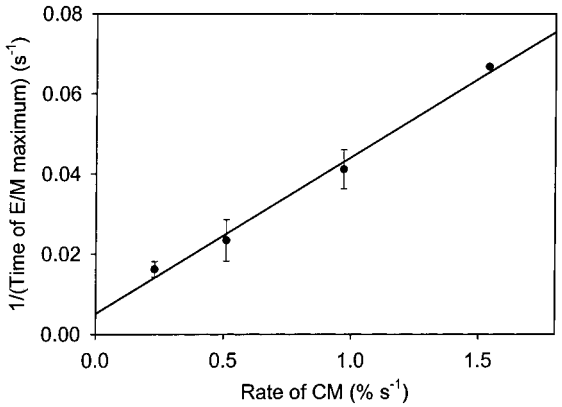

FIGURE 4: Position of the maximum in PY-Ch E/M ratio during DOPC/DOPE/Ch SUV fusion correlates with the initial rate of contents mixing. Measurements of PY-Ch E/M fluorescence and contents mixing were performed in separate experiments at different PEG concentrations (5, 6, 7, and 8 wt %) at 23 °C. Error bars show the standard error of the mean value obtained from 3 independent experiments.

Pyrene Cholesterol Shows the Greatest Excimer Formation during both SUV Fusion and the $L_\alpha-H_{II}$ Transition. The change in E/M ratio of PY-Ch during PEG-induced vesicle fusion was small and could be caused by events other than excimer formation, such as light scattering or a change in pyrene environment and consequent change in the probe quantum yield. To control for such possibilities, we tested different pyrene-containing probes incorporated into SUVs under the conditions for PEG-induced vesicle fusion (Figure 5A). All the data sets were normalized relative to the signal in the control (no PEG) so that the magnitudes of E/M ratios were all comparable. For all four probes, an initial jump (3−4%) in E/M ratio was observed. This jump is probably due to pyrene excimer formation associated with an intermediate that leads to lipid mixing but not fusion (see above). After the jump, PY-PE and PY-HDA showed gradual decreases in E/M ratio, which reached even below the control level, suggesting that these probes were somewhat more dispersed in the fusion product than in the initial SUV population. This would occur if these probes were preferentially distributed to the outer leaflets of SUVs but distributed equally between leaflets in the fusion product. PY-Ch showed the largest and most reproducible increase in E/M ratio, which, as noted previously, was followed by a decrease. With PY-DA, there was also a slight maximum or possibly a delay in the decrease in E/M ratio (Figure 6A).

This special feature of PY-Ch becomes more interesting if we compare its increase in E/M ratio in the H_{II} phase relative to the L_α phase with that of other probes, as summarized in Figure 5B. In Figure 5C, we make a direct comparison of the behaviors of all four probes during PEG-mediated fusion to their behaviors in the H_{II} phase relative to the L_α phase. As we have noted, PY-Ch showed the greatest increase in E/M ratio both in the comparison of lamellar and hexagonal phases and in the fusion studies. PY-DA showed moderate excimer formation in the hexagonal relative to the lamellar phase (Figure 5B), less than PY-Ch but still significantly larger than PY-HDA or PY-PE. This probe was the only other probe that showed any, albeit very small, increase in E/M ratio in the fusing SUV experiments (Figure 5A). Summarizing these results, the correlation between the initial rate of change in E/M ratio in fusing

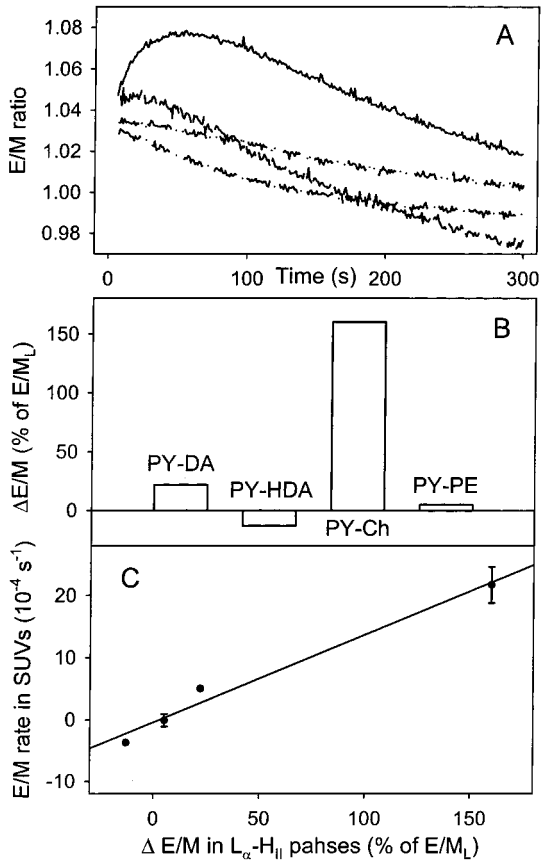

FIGURE 5: Correlation between the extents of excimer formation during SUV fusion and H_{II} formation. (A) Time courses of pyrene E/M ratio change for four probes during PEG (5 wt %)-induced SUV fusion. All probes (PY-Ch, PY-DA, PY-HDA, PY-PE) were at 0.5 mol % in DOPC/DOPE/Ch vesicles. The E/M ratios were normalized to the control without PEG. (B) Increases in pyrene E/M ratios for these four probes in DiPoPE samples in the hexagonal phase relative to the lamellar phase were determined from data shown in Figure 2. (C) Correlation between E/M ratio increase in the H_{II} phase (panel A) and the initial rate of E/M change during fusion of DOPC/DOPE/Ch SUV (panel B).

vesicles and the change in E/M ratio associated with the DiPoPE $L_\alpha-H_{II}$ phase transition (Figure 5C; $R^2 = 0.979$) suggests a clear relationship between the partitioning of these pyrene probes between lamellar and nonlamellar regions in the intermediate states of fusion and the partitioning of them between lamellar and HM regions of the hexagonal phase.

DISCUSSION

We have documented experimentally significant changes in pyrene excimer formation for four lipid probes when lipid bilayers undergo structural rearrangements associated with the fusion process. The behavior of these probes in membrane vesicles induced to fuse by PEG paralleled their behavior in bilayer systems induced to form H_{II} phase by changes in temperature. We know that the H_{II} phase includes lipid monolayers with extremely high curvature and that this high curvature produces regions that cannot be occupied by lipids organized into lamellar structures. Several models have been proposed to describe the structure of these regions (*6*, *7*, *21*). We refer to these regions using the term hydrophobic mismatch (HM), since this term does not relate to any particular model. HM presumably results in a very high free energy so that the normal lamellar lipid organization will distort to reduce this free energy. Our goal in this work was

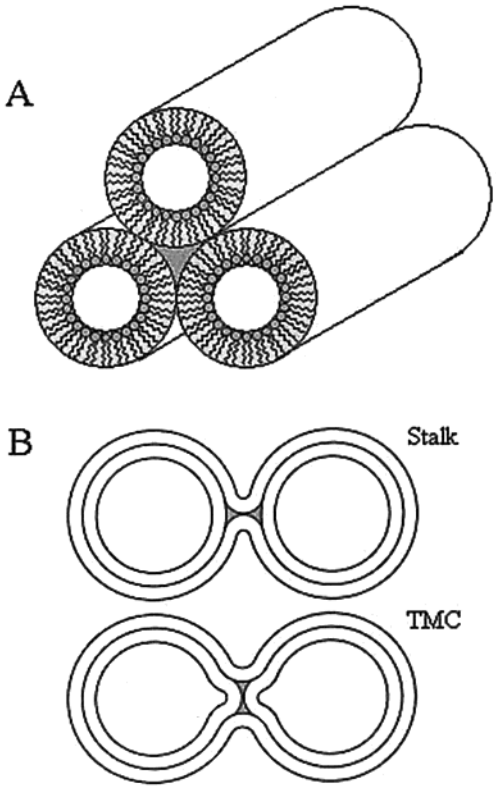

FIGURE 6: Inverted hexagonal phase (A) and fusion intermediates (B). The presumed main intermediates of lipid vesicle fusion are shown: the Stalk and the TMC (trans-membrane contact). The hydrophobic mismatch areas in both the H_{II} phase and presumed fusion intermediates are marked in gray.

to identify a molecule that might identify HM regions and thereby provide a way to monitor formation of HM associated with fusion intermediates produced during the fusion process. The data presented here support two conclusions: (1) PY-Ch and PY-DA both seem to partition into regions of HM within the H_{II} phase, with PY-Ch showing the most dramatic preference for these regions. (2) The PY-Ch E/M ratio seems to mark HM formation and disappearance during PEG-mediated vesicle fusion.

We examine these conclusions in order.

Pyrene Cholesterol Probably Partitions into Regions of HM in the H_{II} Phase. Pyrene and pyrene-labeled probes have been used extensively for studying changes in lipid bilayer and nonbilayer structures and for detecting inhomogeneous distribution of lipids within lamellar phases. Among possible reasons for the changes we have observed in pyrene excimer formation in H_{II} relative to the lamellar phase, we can imagine the following: (1) change in probe lateral mobility (diffusion coefficient) due to a uniform change in lipid packing; or (2) nonuniform probe distribution, which in turn could be within the lipid monolayer or between monolayer and HM.

The probability of dynamic excimer formation increases with the diffusion coefficient (*19*). We can see this in our data as E/M increases with temperature (Figure 2). Thus, the increase in E/M that we see in the H_{II} phase could reflect faster probe diffusion than in the lamellar phase. Using PY-PC as a probe, Chen et al. found that the lateral diffusion of lipids in the DOPE H_{II} phase is lower than in the L_α phase at the same temperature (*3*). Our results also indicate that the effect we have observed is probably not due to a uniform change in physical properties of the lipid phase (e.g., a uniform change in lipid packing resulting in a change in diffusion coefficient). Such a uniform change in lipid environment should affect diffusion of all the probes similarly, leading to similar changes in E/M, which is not what we observed.

Of course, events that produce inhomogeneous changes in lipid packing and thus lead to an inhomogeneous distribution of probe will affect different probes differently, just as we have observed. Such events would produce locally increased probe concentrations, which would increase the probability of excimer formation and the observed E/M ratio, and could alter local diffusional rates in ways that might increase or decrease E/M. Thus, we conclude that the increase in excimer formation for PY-DA and PY-Ch that we see upon forming H_{II} from the lamellar phase is most likely due to a less uniform probe distribution in the H_{II} relative to the lamellar phase. Of the four pyrene probes examined, PY-Ch seems to redistribute and accumulate most readily in some regions associated with the inverted hexagonal phase. Are these regions likely to be ones of high monolayer curvature or regions of HM caused by the failure of the curved monolayers to pack well into a hexagonal array?

According to the conventional model for the inverted hexagonal phase as rows of cylindrical tubes with water inside (see Figure 6A), the curvature of the lipid monolayer component is constant along the perimeter of the tube. Thus, there should not be any preference for PY-Ch to accumulate preferentially in any particular region in the lamellar structures within the H_{II} phase. If this model is correct, it suggests that PY-Ch accumulates in the regions of HM (see gray areas in Figure 6A) rather than in the highly curved lamellar regions. Another model for the hexagonal phase is one in which the monolayers are not homogeneously bent into cylinders but are roughly flat in the contact regions with higher bending or tilt deformation in the HM region (*6*). In this view, PY-Ch may accumulate not in interstitial spaces but in the lipid phase in the regions of highest packing distortion associated with tilt deformation in the hexagonal phase. No matter which model we adopt to describe the hexagonal phase, the implication of our results is that PY-Ch accumulates in local regions of the hexagonal phase where lipid packing is defective and helps to fill these packing defects. These are by definition what we refer to as HM regions. If this is true, then the accumulation of these probes into HM regions should stabilize the hexagonal phase. This is consistent with the dramatic influence that PY-Ch had on the hysteresis in the H_{II} to L_α cooling transition (Figure 1).

PY-Ch Seems To Mark Regions of HM during Fusion. This interpretation derives from two observations. First, there was a distinct correlation between the initial rate of contents mixing during fusion and the rate of appearance of a maximum in the PY-Ch E/M ratio during PEG-mediated vesicle fusion (Figure 4). This suggests that these observables are related either to a common physical event or to events that are themselves highly correlated. Second, a correlation between the rate of change in E/M ratios of the four probes examined during PEG-mediated vesicle fusion and the extent of change in their E/M ratios in H_{II} relative to the lamellar phase (Figure 5C) suggests that the origin of these changes may be similar in these two systems. Our first conclusion was that a large increase in E/M ratio during the lamellar-to-hexagonal phase transition likely reflects partitioning of PY-Ch into regions of HM in the H_{II} phase. Thus, it is very

likely that the increase in E/M ratio seen during PEG-mediated fusion also reflects partitioning of PY-Ch into regions of HM in nonlamellar structures widely thought to exist in the intermediates leading to pore formation during the fusion process (*8*, *9*, *22*) (Figure 6B). This is not to suggest that PY-Ch actually "fills voids", just that it seems to have a molecular shape and polarity that allow it to relieve the packing stresses that accompany formation of local regions of nonlamellar structure in lipid mixtures that prefer a lamellar packing arrangement.

Relationship of Our Observations to the Fusion Mechanism. We have recently reported an analysis of the kinetics of PEG-mediated fusion that demonstrates two intermediate states (*9*). A small region of HM occurs in the initial intermediate (called I1 and often viewed as the "stalk" shown in Figure 6B), which forms rapidly, is reversible, and is associated with lipid exchange but not pore formation (*9*). The intermediate that forms later in the PEG-mediated fusion process (called I2 and possibly the TMC in Figure 6B) (*9*) also has regions of HM (also gray shaded region in Figure 6B), which provide a free energy barrier to pore formation (*10*). Pore formation returns the system to a purely lamellar state and eliminates the HM, thus completing the fusion process. In this view of the fusion process, which is in broad terms currently widely accepted, one expects to see an initial increase in regions of HM followed by disappearance of these as the process completes with pore formation. Since the PY-Ch E/M ratio appears to mark HM, we would expect to see this ratio increase with formation of initial and secondary intermediates and then decrease as pore formation occurs. This is exactly what we observed. However, the time courses for the PY-Ch E/M ratio in different lipid systems suggest either that the PY-Ch E/M ratio detects more than I1 or that lipid mixing does not occur instantaneously within the I1 state. In DOPC/DOPE/Ch and DOPC/DOPE SUVs, there was a very rapid increase in this ratio from a value of 1 seen in the absence of PEG (Figure 3A). This occurred much more rapidly than did lipid mixing (Figure 3B), meaning that PY-Ch redistributed roughly as soon as the vesicles were aggregated by PEG, but that lipids then redistributed between vesicles by a slower process. The rapid increase in E/M ratio seems to mark a state in which lipids *can* redistribute between vesicles, since no increase was seen in SOPC SUVs for which no lipid mixing was observed. We have previously defined I1 as the state in which lipid mixing can occur (*9*). Why do we now find that lipid mixing is much slower than formation of this state, contrary to what we have previously assumed (*9*)? This may be because lipid diffusion through I1 is much slower than lateral diffusion within a bilayer, or it may be because, as we have concluded previously (*9*), two types of interbilayer contact occur, one that allows for lipid transfer between vesicles and one that does not. The rate of lipid mixing would then be proportional to the concentration of contacts times the fraction of contacts that result in the I1 state. If this fraction is small and fairly constant, then lipid mixing would proceed at a steady rate much slower than the rate at which I1 contacts initially formed.

Whatever the explanation for the rate of lipid mixing is, it is interesting that, in DOPC/DOPE SUVs that did not fuse, the state marked by a high E/M ratio decayed at a slow rate that was comparable to that at which lipids redistributed between vesicles. If this state represents I1, then I1 can decay by lipid rearrangements other than those that lead to pore formation. In DOPC/DOPE/Ch SUVs, the increase of the E/M ratio after formation of this initial state seems to mark formation of a structure (I2) capable of forming a pore. This suggestion follows from the fact that this rise was seen only under conditions for which fusion occurred, and from the fact that formation of this higher E/M state occurred more rapidly the more rapidly contents mixing occurred (Figure 4). These observations indicate that local increases in PY-Ch concentration mark some aspect(s) of the fusion process. Our current interpretation is that accumulation of PY-Ch marks the intermediate structures that lead to pore formation (Figure 3), whatever may be their detailed structure, and thus provides a tool for monitoring fusion intermediates. However, additional testing in terms of a detailed kinetic model and rapid mixing kinetics will be needed to fully test this interpretation.

REFERENCES

1. Barenholz, Y., Gibbes, D., Litman, B. J., Goll, J., Thompson, T. E., and Carlson, R. D. (1977) *Biochemistry 16*, 2806−2810.
2. Chen, P. S., Jr., Toribara, T. Y., and Warner, H. (1956) *Anal. Chem. 28*, 1756−1758.
3. Chen, S. Y., Cheng, K. H., and Ortalano, D. M. (1990) *Chem. Phys. Lipids 53*, 321−329.
4. Chernomordik, L. V., Frolov, V. A., Leikina, E., Bronk, P., and Zimmerberg, J. (1998) *J. Cell Biol. 140*, 1369−1382.
5. Epand, R. M. (1990) *Chem. Phys. Lipids 52*, 227−230.
6. Hamm, M., and Kozlov, M. M. (1998) *Eur. Phys. J. B 6*, 519−528.
7. Kirk, G. L., Gruner, S. M., and Stein, D. L. (1984) *Biochemistry 23*, 1093−1102.
8. Kozlov, M. M., Leikin, S. L., Chernomordik, L. V., Markin, V. S., and Chizmadzhev, Y. A. (1989) *Eur. Biophys. J. 17*, 121−129.
9. Lee, J., and Lentz, B. R. (1997) *Biochemistry 36*, 6251−6259.
10. Lee, J., and Lentz, B. R. (1998) *Proc. Natl. Acad. Sci. U.S.A. 95*, 9274−9279.
11. Lentz, B. R., Carpenter, T. J., and Alford, D. R. (1987) *Biochemistry 26*, 5389−5397.
12. Lentz, B. R., and Lee, J. K. (1999) *Mol. Membr. Biol. 16*, 279−296.
13. Lentz, B. R., Malinin, V., Haque, M. E., and Evans, K. (2000) *Curr. Opin. Struct. Biol. 10*, 607−615.
14. Lentz, B. R., McIntyre, G. F., Parks, D. J., Yates, J. C., and Massenburg, D. (1992) *Biochemistry 31*, 2643−2653.
15. Lentz, B. R., Talbot, W., Lee, J., and Zheng, L. X. (1997) *Biochemistry 36*, 2076−2083.
16. Malinin, V. S., Frederik, P., and Lentz, B. R. (2001) *Biophys. J. 82*, 2090−2100.
17. Malinin, V. S., Haque, M. E., and Lentz, B. R. (2001) *Biochemistry 40*, 8292−8299.
18. Massenburg, D., and Lentz, B. R. (1993) *Biochemistry 32*, 9172−9180.
19. Sassaroli, M., Vauhkonen, M., Perry, D., and Eisinger, J. (1990) *Biophys. J. 57*, 281−290.
20. Schwenk, E., and Werthessen, N. T. (1952) *Arch. Biochem. Biophys. 40*, 334−341.
21. Siegel, D. P. (1993) *Biophys. J. 65*, 2124−2140.
22. Siegel, D. P. (1999) *Biophys. J. 76*, 291−313.
23. Siegel, D. P., and Epand, R. M. (1997) *Biophys. J. 73*, 3089−3111.
24. Talbot, W. A., Zheng, L. X., and Lentz, B. R. (1997) *Biochemistry 36*, 5827−5836.
25. Turner, D. C., and Gruner, S. M. (1992) *Biochemistry 31*, 1340−1355.
26. Wilschut, J., Duzgunes, N., Fraley, R., and Papahadjopoulos, D. (1980) *Biochemistry 19*, 6011−6021.

BI011924H